Journal of Power Sources 253 (2014) 193–200

Contents lists available at ScienceDirect

Journal of Power Sources

journal homepage: www.elsevier.com/locate/jpowsour

Nitrogen-doped carbon coated TiO_2 nanocomposites as anode material to improve cycle life for lithium-ion batteries

Lei Tan [a], Lei Pan [a], Chengying Cao [a], Baofeng Wang [b], Lei Li [a,*]

[a] School of Chemistry and Chemical Engineering, Shanghai Jiaotong University, Shanghai 200240, China
[b] Shanghai University of Electric Power, Shanghai 200090, China

HIGHLIGHTS

- Polydopamine used as carbon precursor to prepare carbon coated TiO_2 composite.
- The effect of the carbon layer thickness of the lithium-ion battery is investigated.
- The optimized thickness of the carbon layer is about 4–5 nm.
- The lithium-ion battery using carbon coated TiO_2 shows good cyclability.

ARTICLE INFO

Article history:
Received 24 October 2013
Received in revised form
28 November 2013
Accepted 12 December 2013
Available online 19 December 2013

Keywords:
Titanium dioxide
Carbon coating
Polydopamine
Lithium-ion battery
Cycle life

ABSTRACT

Anatase TiO_2 has attracted much attention as a safe anode material for lithium-ion battery applications, due to its low electronic conductivity and severe aggregation during Li^+ insertion/extraction processes, the practical application of the anatase TiO_2 is still hindered by poor long-term cycling stability. In order to improve the cycling performance of lithium-ion batteries, a uniform thin nitrogen-doped carbon layer with a thickness of 3–6 nm is successfully coated on the surface of the anatase TiO_2 nanoparticles by using polydopamine as carbon precursor. Compared with the pristine TiO_2 electrode, the carbon coated TiO_2 nanocomposites electrodes show very good capacity retention and cycling performance.

1. Introduction

TiO_2 materials have been actively studied as a typically safe anode material in lithium-ion batteries (LIBs) due to its natural abundance, low cost, environmentally friendliness, biocompatibility and superior safety [1,2]. In comparison to the other polymorphs of TiO_2, anatase TiO_2 is generally considered as the most electroactive Li-insertion host, because it not only has a low voltage (1.7 V versus Li/Li^+) insertion host for Li^+, but also shows fast Li^+ insertion/extraction kinetics [1,2]. However, due to severe aggregation during Li^+ insertion/extraction processes, the practical application of anatase TiO_2 is still hindered by poor long-term cycling stability. Moreover, the low electronic conductivity of TiO_2 itself often further hastens the degradation process.

To improve the cycling performance of TiO_2, the nano-scale coating on the surface of TiO_2 nanoparticles has been explored. Depending on the nature of the coating materials, the surface coating can promote faster Li^+ ion diffusion and/or electron transport, suppress the nanoparticles clustering and limit excessive particle growth. A number of the coating materials, such as Ag, Sn, Cu, P, SiO_2, V_2O_3 and carbon have been developed [3–10]. Some core–shell nanostructured materials have been widely explored for Li ion batteries [11–14]. Among these coating materials, carbon draws special attention since it can provide conductive electronic path leading to higher electronic conductivity. Carbon coating can be synthesized easily by using a variety of methods, such as hydrothermal or solvothermal synthesis [8], sol–gel process [9], and chemical vapor deposition (CVD) methods [10]. However, these methods also suffer from one or other drawbacks regarding their complex or multiple stages, rigorous reaction conditions or unstable precursors. For example, the sol–gel processing usually demands precise control reaction conditions, such as pH, temperature or the

* Corresponding author. Tel.: +86 21 34202613; fax: +86 21 54742567.
E-mail address: lilei0323@sjtu.edu.cn (L. Li).

0378-7753/$ – see front matter © 2013 Elsevier B.V. All rights reserved.
http://dx.doi.org/10.1016/j.jpowsour.2013.12.059

presence of anions or surfactants in the reaction system. The CVD method requires special and expensive equipments, which will increase the production cost. The hydrothermal method needs extreme conditions, such as high temperature and high pressure. In addition, it is still a big challenge to coat a uniform, continuous and controllable thickness of carbon layer on the surface of TiO_2 nanoparticles based on these methods mentioned above. The uniform and continuous carbon layer can provide rapid and continuous electronic transport and prevent the direct contact between TiO_2 and electrolyte, which will avoid capacity fading and safety problems. The optimized thickness of carbon layer can also prevent the TiO_2 nanoparticles clustering and improve the performance of LIBs.

Herein we report a facile method to prepare nitrogen-doped carbon coated TiO_2 (TiO_2@C) nanoparticles by using polydopamine (PODA) as carbon precursor (see Scheme 1). The PODA, one of nature-inspired materials, is a component found in mussel adhesive proteins (MAPs). Mimicking MAPs, dopamine, a biomolecule that contains catechol and amine functional groups, can self-polymerize in weak alkaline aqueous solution and spontaneously deposit the PODA films on virtually any surfaces such as bulk substrates and nanostructures [15]. Due to the strong and versatile coating capability of the PODA polymer, it will be easy to form a uniform and continuous the PODA coating film on the nanoparticle surface. The thickness of such the PODA coating film could also be precisely controlled from a few nanometers to 50 nm through varying the polymerization time. Since the PODA containing N species, the nitrogen-doped carbon layer will be obtained after the calcination treatment. It has been reported that the N-doping carbon will improve the cycling performance of metal oxide-carbon composites due to the improvement in electronic conductivity, Li^+ ion permeability of the carbon layer, charge transfer at the interface and stability of the SEI films [16]. Carbonized the PODA has been successfully used as an Au nanoparticles support for catalytic application as well as in capacitors [17]. Recently, the carbonized PODA coating on the surface of Fe_3O_4 nanostructures used as lithium-ion battery anodes have been prepared [18]. More recently, we prepared the N-doped carbon layer (thickness of 4 nm) coated TiO_2 nanocomposites by using the PODA as carbon precursor, and found that the lithium-ion battery using this nanocomposites showed good capacity retention compared with the battery using the pristine TiO_2 [19]. In general, the carbon layer thickness will directly affect the electrochemical performance of the core–shell nanostructured materials in the LIBs, such as cycling stability and specific capacity. In this paper, we prepared the TiO_2@C nanocomposites with the different carbon layer thickness of 3–6 nm by using the PODA as carbon precursor. The effect of the carbon layer thickness on the lithium-ion battery is investigated via a combination of cyclability, electrochemical impedance spectroscopy (EIS) and scanning electron microscope (SEM).

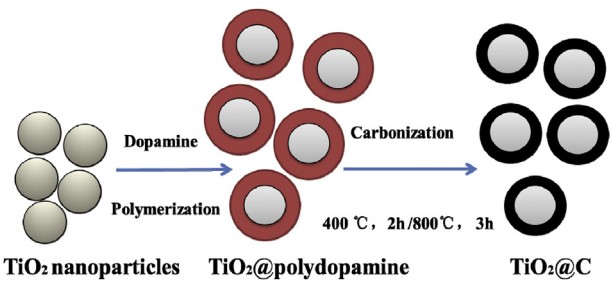

Scheme 1. Illustration of the preparation of nitrogen-doped carbon coated TiO_2 nanocomposites by using polydopamine as carbon precursor.

2. Experimental

2.1. Chemicals

Anatase TiO_2 nanoparticles and dopamine hydrochloride were purchased from Aladdin Industrial Corporation. Battery-grade ethylene carbonate (EC), dimethyl carbonate (DMC) and $LiPF_6$ were purchased from Shenzhen Capchem Chemicals Co., Ltd., China, and used without further purification.

2.2. Synthesis of TiO_2@C composites

Typically, 200 mg anatase TiO_2 nanoparticles were dispersed in 100 mL tris-buffer (pH: ~8.5) by ultrasonication for at least 30 min to form a suspension. Subsequently, 200 mg dopamine was added to the mixture under stirring at room temperature. Afterward, the precipitates were collected by centrifugation, washed three times with deionized water, and then dried at 80 °C for 10 h. To carbonize the polydopamine coating, the dried powders were placed in a tube and heated to 400 °C at a rate of 1 °C min^{-1} under Ar atmosphere and kept this temperature for 2 h, and then heated to 800 °C with a heating rate of 5 °C min^{-1}, and kept at 800 °C for 3 h. The obtained composites were donated as TiO_2@C. Here, we report TiO_2@C nanocomposites samples with different polymerization time: 5 h for TiO_2@C-1, 10 h for TiO_2@C-2 and 24 h for TiO_2@C-3, respectively.

2.3. Characterization

Transmission electron microscopy (TEM) analysis was carried out with a Tecnai G220S-Twin equipment operating at 200 kV. X-ray diffraction (XRD) measurements were taken on an X-ray diffractometer (XRD, D/max-2200/PC, Japan) by continuous scanning in the 2θ range of 10–80°. The chemical composition of the polydopamine coated TiO_2 nanocomposites was analyzed by Fourier transform infrared spectroscopy (ATR-FTIR, Spectrum 100, Perkin Elmer, Inc., USA). X-ray photoelectron spectroscopy (XPS) measurements were carried out by a Kratos Axis UltraDLD spectrometer (Kratos Analytical-A Shimadzu group company) using a monochromatic Al Kα radiation ($h\gamma = 1486.6$ eV). The binding energies of the samples were calibrated by taking the carbon 1s peak as a reference (284.6 eV). The weight content of TiO_2 and carbon in the TiO_2@C composites was determined from the weight loss curve measured under simulated air atmosphere on a TG/DTA instrument (PerkinElmer) with a heating rate of 10 °C min^{-1}. Scanning electron microscope (SEM, Ultra 55, Carl Zeiss) was used to observe the morphology of TiO_2 and TiO_2@C composites electrodes. Electron conductivity of TiO_2 and TiO_2@C composites was measured with AC impedance method by using Autolab PGSTAT302 electrochemical test system (Eco Chemie, the Netherlands) at room temperature. The TiO_2 and TiO_2@C composites pellets were prepared by pressing the corresponding powders at 20 MPa. The electron conductivity was calculated from impedance data.

2.4. Electrochemical measurements

Electrochemical experiments were carried out via CR2016 cointype test cells assembled in an argon-filled glove box with lithium metal as the counter and reference electrodes. The working electrodes were prepared by mixing TiO_2 or TiO_2@C composites, carbon black, and sodium carboxymethyl cellulose at a weight ratio of 70:20:10. After magnetic stirring, the resulting slurries were immediately casted onto copper foil, dried in oven at 80 °C for 2 h, and then left at room temperature overnight. Circular electrodes with a diameter of 12 mm were punched and subsequently dried at 80 °C under vacuum for 24 h. A Celgard 2400 membrane was used

as a separator. The electrolyte consisted of a solution of 1 M $LiPF_6$ in a 1:1 (v/v) EC/DMC. The discharge–charge measurements were performed on Land CT2001A tester (Wuhan, China) at the constant current mode over the range of 1.0–3.0 V. The constant current mode of 0.5 C (0.08 A g^{-1}) was carried out at room temperature. Electrochemical impedance spectroscopy (EIS) of the cell was observed immediately under full charged condition. EIS measurement was accomplished by coupling the potentiostat with an Autolab frequency response analyzer locked in an amplifier and an impedance phase analyzer. A sinusoidal amplitude modulation was used over the frequency range from 0.1 Hz to 1 MHz.

3. Results and discussion

N-doped carbon coated TiO_2 nanocomposites were prepared through a two-step method shown in Scheme 1. First, the PODA layer was spontaneously coated onto the surface of anatase TiO_2 nanoparticles (about 50 nm, see Fig. 1a) through the self-polymerization of dopamine in Tris-buffer (pH 8.5) aqueous solution at room temperature. Subsequently, the PODA layer was converted into carbon layer by calcination in nitrogen atmosphere at 800 °C. Through such process, core–shell TiO_2@C nanocomposites with inner anatase TiO_2 nanoparticle and an outer carbon shell were obtained. In Fig. 1, it can be observed that anatase TiO_2 nanoparticles were coated with a uniform thin carbon layer with a thickness of 3–6 nm. And the thickness of such N-doped carbon layers can be precisely controlled through varying the polymerization time of the PODA polymers in our experiments.

The PODA coating on the surface of TiO_2 nanoparticles was confirmed by Fourier transform infrared spectroscopy (FTIR) measurements. Compared with the pristine TiO_2, some new peaks appeared in the TiO_2@PODA composites (Fig. 2): the peaks at 1509 cm^{-1} ascribed to the N–H shearing vibration of the amide group, and the peaks at 1442 cm^{-1} and 1294 cm^{-1} attributed to the C–C vibration of the benzene ring moiety and the phenolic C–OH stretching vibration, respectively [20]. Fig. 3 shows the X-ray diffraction (XRD) patterns of the anatase TiO_2 and TiO_2@C nanocomposites. In contrast, the diffraction peaks of the TiO_2@C nanocomposites are similar to the pristine anatase TiO_2 (JCPDS, card no: 21-1272). Previously, it has been reported that the phase transformation of pure anatase to rutile occurs at around 600 °C [21]. Our XRD data, however, demonstrate that the anatase phase, when coated with carbon shell, can be sustained above this transformation temperature even when the reaction was conducted at 800 °C in an inert atmosphere. The suppression of the phase transition has been attributed to the presence of a carbon shell around the TiO_2 nanoparticle, which is consistent with the reported results in the other groups [21].

The chemical information of the TiO_2@C nanocomposites was examined by X-ray photoelectron spectroscopy (XPS) measurements shown in Fig. 4. Due to the carbon coating layer, the intensity of both O1s and Ti2p peaks were decreased and the intensity of C1s peak increased compared with the pristine TiO_2. In addition, one new peak of N1s appeared in the TiO_2@C composites, which indicates that the carbon coating layer is nitrogen-doped. The weight content of nitrogen is calculated to be 7.96 wt% according to the XPS measurements. From the high-resolution XPS spectra of N1s for TiO_2@C (Fig. 4(b)), it can be seen that the N1s region exhibits three main contributions: the peak at 398.3 eV belongs to pyridinic nitrogen (N1), the peak at 399.5 eV belongs to pyrrolic nitrogen (N2), and the peak at 400.3 eV indicates the presence of quaternary nitrogen (N3). The minor N1s peak at 402.4 eV (N4) originates from the N-oxide of pyridinic nitrogen. It will benefit the electrochemical performance of the TiO_2@C composites in the lithium-ion battery, since the nitrogen-doping has been reported to facilitate the electronic conductivity of the carbon layer and the charge transfer at the interface [16,22,23].

The carbon layer thickness (the carbon content) will directly affect the electrochemical performance of TiO_2 nanoparticles in the LIBs, including cycling stability and specific capacity. When the carbon layer is too thin, it is difficult to form a buffer layer which is strong enough to suppress the TiO_2 nanoparticle clustering and limit excessive TiO_2 particle growth. Conversely, when the carbon layer is too thick, the specific capacity of the composites may decrease because of the restricted efficient ion transfer/transport. Therefore, it is important to obtain a carbon layer with optimized thickness. As shown in Fig. 1, the carbon layer thickness can be controlled by the polymerization time of the PODA in our experiments. Then, we prepared some TiO_2@C nanocomposites with different thickness of carbon layer by varying the polymerization time: 5 h for TiO_2@C-1 (3 nm), 10 h for TiO_2@C-2 (4 nm) and 24 h for TiO_2@C-3 (6 nm), respectively. The carbon content is determined by thermogravimetric analysis. As shown in Fig. 5, a weight loss below 150 °C is attributed to the evaporation of the absorbed moisture, and a major weight loss takes place between 250 and 550 °C, giving rise to an observed weight loss of 3.0 wt%, 4.2 wt% and 12.7 wt% for TiO_2@C-1, TiO_2@C-2 and TiO_2@C-3, respectively. Due to the N-doped carbon layers coating on the TiO_2 nanoparticles, the electronic conductivity increased compared with the pristine TiO2 nanoparticles. In our experiments, the electron conductivity of TiO_2, TiO_2@C-1, TiO_2@C-2 and TiO_2@C-3 was 2.66×10^{-5} S cm^{-1}, 1.353×10^{-4} S cm^{-1}, 2.422×10^{-4} S cm^{-1} and 6.027×10^{-4} S cm^{-1}, respectively.

The cycling performance of the TiO_2 and TiO_2@C electrodes were shown in Fig. 6. The cells were cycled at 0.5 C under constant current conditions at room temperature. Compared with the first cycle capacity of the TiO_2 (151.3 mAh g^{-1}), the first cycle capacity of both TiO_2@C-1 (155.7 mAh g^{-1}) and TiO_2@C-2 (160.9 mAh g^{-1}) electrodes show higher values, however, TiO_2@C-3 (132.7 mAh g^{-1}) electrode with the thick carbon layer has lower value. It can be found that the cycling performance of the TiO_2@C electrodes was better than that of the pristine TiO_2 electrode. The capacity fading of the TiO_2 electrode was severe, and the capacity declined to 81.1 mAh g^{-1} (capacity retention: 53.6%) after 170th cycles. As for the TiO2@C electrodes after 170th cycles, the capacity decreased to 127.3 mAh g^{-1} (capacity retention: 81.8%), 142.4 mAh g^{-1} (capacity retention: 88.5%) and 131.4 mAh g^{-1} (capacity retention: 99.0%) for TiO_2@C-1, TiO_2@C-2 and TiO_2@C-3 electrodes, respectively. The discharge–charge voltage profiles of the TiO_2 and TiO_2@C nanocomposites for the 1st, 10th, 100th and 170th cycles are shown in Fig. 7. The comparison of these voltage profiles of all electrodes at the same rate indicates that the superior electrochemical performance of TiO_2@C based electrodes, particularly TiO_2@C-2 composites, results from the significantly reduced capacity loss per cycle. Due to the reduced aggregation of active particles and an enhanced electron conductivity caused by the carbon layer, TiO_2@C based electrodes show more stable discharge–charge voltage profiles than that of the pure anatase TiO_2. As can be seen in Fig. 7, the capacity fading of the pristine anatase TiO_2 based electrode is more pronounced than that of the TiO_2@C based electrodes. The similar behavior has also been reported in the literature. For example, Zhou et al. prepared TiO_2/reduced graphene oxide (TiO_2/RGO) nanosheets, and found that the TiO_2/RGO nanosheets showed good cycling performance than that of the pristine TiO_2 electrode in lithium-ion battery [24].

These behaviors are attributed to the carbon coating layers. Without the carbon layer on the TiO_2 nanoparticles, these anatase TiO_2 nanoparticles show severe aggregation after cycling (Fig. 8a and b), which will further hinder the lithium-ion transport and destroy the stability of SEI films, and then results in a significant capacity

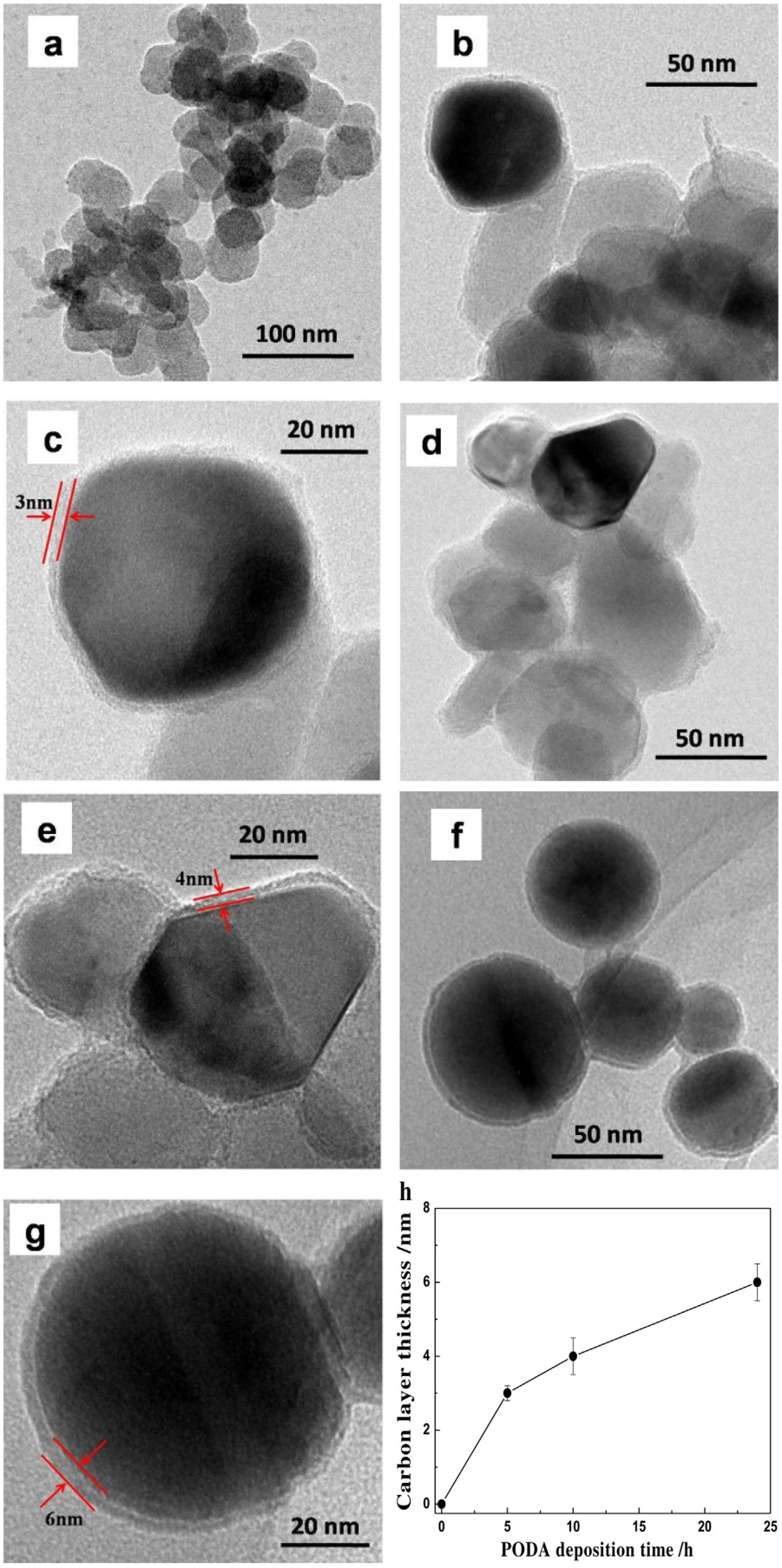

Fig. 1. TEM images of (a) pristine anatase TiO_2, and TiO_2@C nanocomposites for 5 h (b) and (c), 10 h (d) and (e), 24 h (f) and (g), respectively. (h) The relationship between the polymerization time of polydopamine and carbon shell thickness of TiO_2@C nanocomposites.

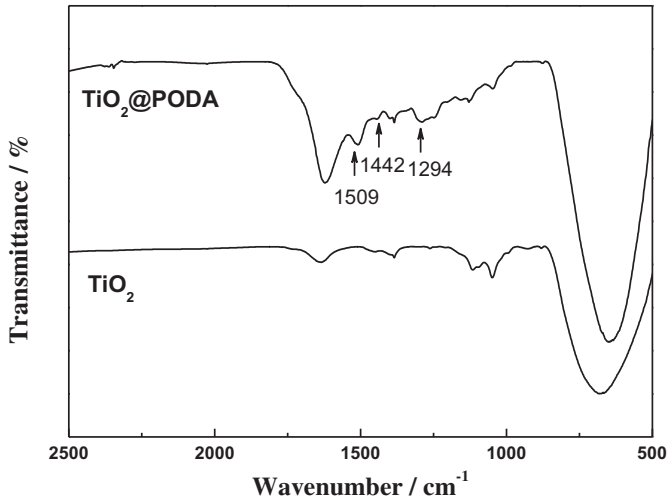

Fig. 2. FTIR spectra of TiO_2 and TiO_2@polydopamine nanocomposites (10 h of polymerization time).

fading. Due to the protective effect of the carbon coating layers, it will suppress the TiO_2 nanoparticles clustering, limit excessive TiO_2 nanoparticles growth and enhance the stability of SEI films (Fig. 8c–h). Compared to TiO_2@C-2 and TiO_2@C-3 electrodes (Fig. 8), TiO_2@C-1 with thin carbon layer (about 3 nm) electrode shows more aggregation of the TiO_2 nanoparticles after cycling. The main reason is the thin carbon layer (about 3 nm) is difficult to form a strong buffer layer to suppress the TiO_2 nanoparticle clustering and limit excessive TiO_2 nanoparticle growth. Nyquist plots obtained from EIS measurements of TiO_2 and TiO_2@C electrodes under full charged condition after 170 cycles are shown in Fig. 9. The spectra exhibits a semicircle in the high-to-medium frequency region followed by a straight slopping line in the low-frequency region. The proposed equivalent circuit for this cell system is depicted in the inset of Fig. 9, where R_s is the ohmic resistance of electrolyte, membrane and electrode, corresponding to the high frequency intercept of the semicircle with the horizontal axis; C_{SEI} and R_{SEI} are the capacitance and the resistance of the solid-electrolyte interface layer, C_d and R_{ct} (the double layer capacitance and the charge transfer resistance, respectively) are related to the semi-circular arc; and W_f (the

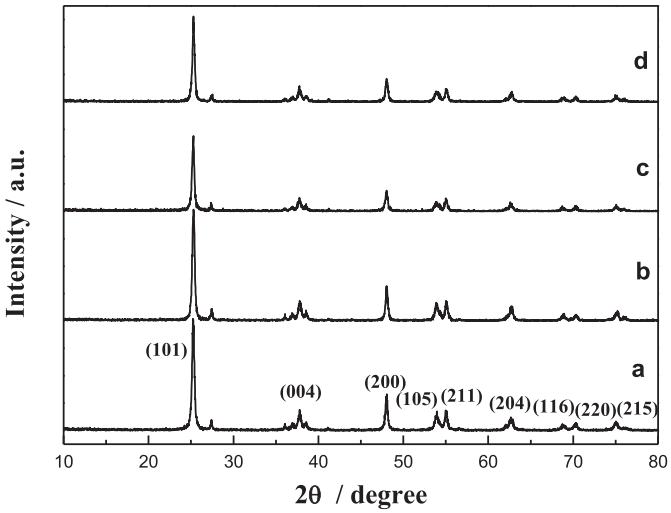

Fig. 3. X-ray diffraction patterns of (a) TiO_2, and TiO_2@C nanocomposites as the self-polymerization of dopamine for 5 h (b), 10 h (c) and 24 h (d), respectively.

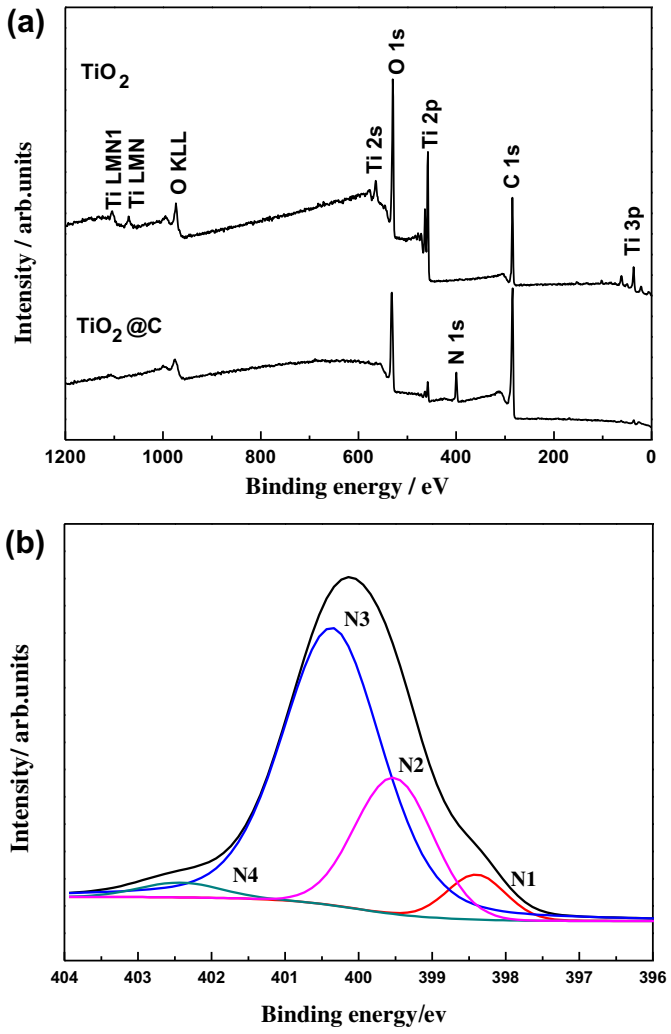

Fig. 4. (a) XPS spectra of TiO_2 and TiO_2@C nanocomposites as the self-polymerization of dopamine for 24 h, (b) N1s spectra of TiO_2@C nanocomposites.

Warburg impedance) corresponds to the straight slopping line at low frequency [3]. The values of charge transfer resistance for TiO_2, TiO_2@C-1, TiO_2@C-2 and TiO_2@C-3 are 107.7 Ω, 82.6 Ω, 44.8 Ω, and 54.8 Ω, respectively. Compared with the pristine TiO_2 nanoparticles,

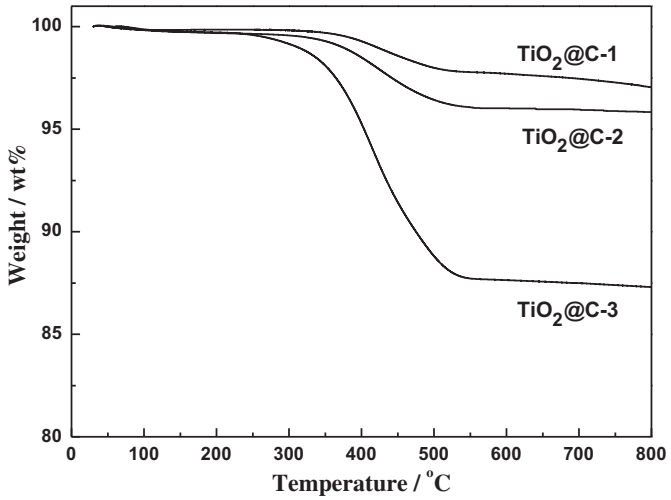

Fig. 5. TG curves of TiO_2@C nanocomposites.

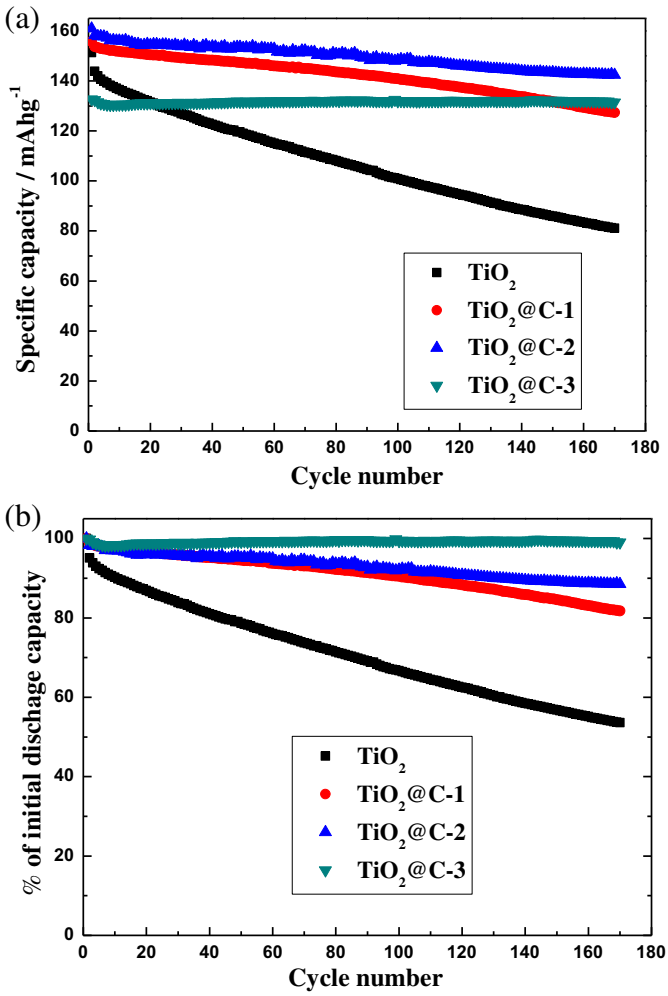

Fig. 6. Discharge capacity (a) and capacity retention (b) versus cycle number plots of TiO_2 and TiO_2@C nanocomposites. Rate: 0.5 C.

the value of R_{ct} is markedly decreased after the carbon coating on the TiO_2 nanoparticles. The value of R_{ct} was ordered: TiO_2@C-2 < TiO_2@C-3 < TiO_2@C-1 < TiO_2. Due to the presence of the conductive N-doped carbon layer, the TiO_2@C electrodes exhibit lower resistance than that of the pristine TiO_2 electrode. Although the TiO_2@C-3 nanocomposite showed the highest electron conductivity mentioned before, it is interesting to find that the lowest R_{ct} value of all the TiO_2@C electrodes is obtained for the TiO_2@C-2 electrode in our experiments. Maybe the main reason is the different structures of these electrodes including the SEI film and TiO_2@C nanocomposite after cycling.

The diffusion coefficient D of lithium ion can be calculated from plots in the low-frequency region according to the following equation [25,26]:

$$D = R^2T^2/2A^2n^4F^4C^2\sigma^2 \quad (1)$$

where R is the gas constant, T is the absolute temperature, n is the number of electron(s) per molecule oxidized, A is the surface area, F is Faraday's constant, C is the concern concentration, and σ is the Warburgfactor which has relationship with Zre as follows:

$$\mathrm{Zre} = R_{ct} + R_s + \sigma\omega^{-1/2} \quad (2)$$

Based on Eqs. (1) and (2), the values of diffusion coefficient of TiO_2, TiO_2@C-1, TiO_2@C-2 and TiO_2@C-3 are 4.63×10^{-13} cm^2 s^{-1},

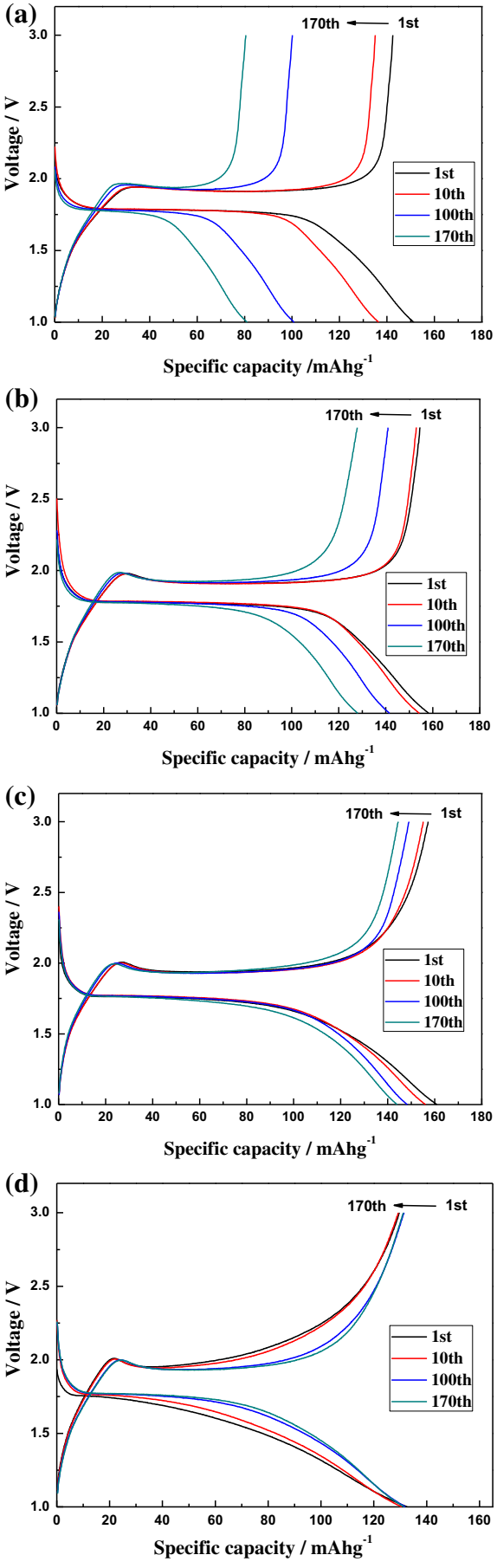

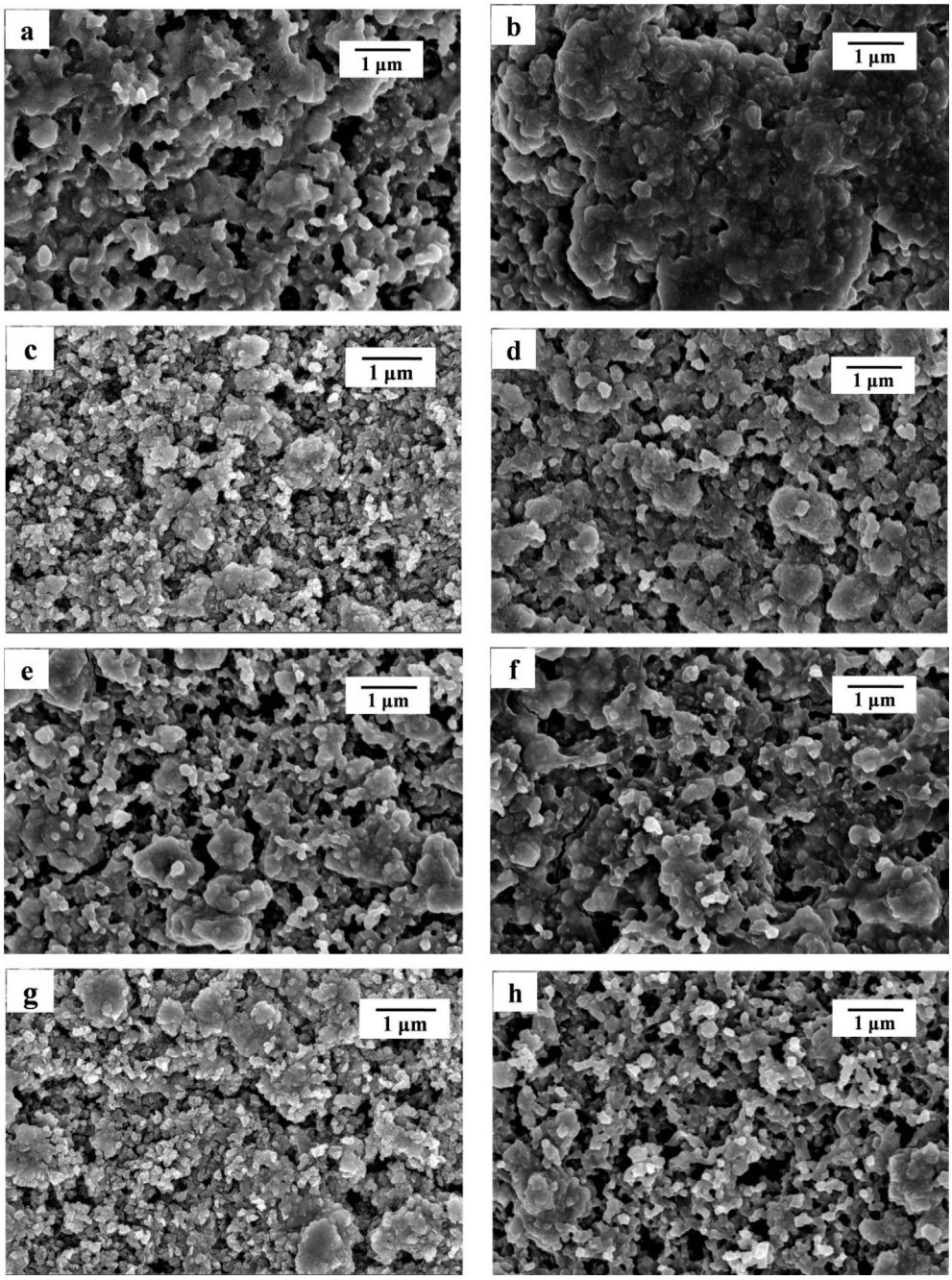

Fig. 8. SEM images of electrodes after the first cycle: (a) TiO_2, (c) TiO_2@C-1, (e) TiO_2@C-2, (g) TiO_2@C-3, and 170th cycles: (b) TiO_2, (d) TiO_2@C-1, (f) TiO_2@C-2, (h) TiO_2@C-3.

7.49×10^{-13} $cm^2 s^{-1}$, $3.08^{-} \times {}^{-}10^{-12}$ $cm^2 s^{-1}$ and 1.53×10^{-12} $cm^2 s^{-1}$, respectively. Compared with the pristine TiO_2 nanoparticles, the value of the diffusion coefficient of Li^+ ion is increased after the carbon coating on the TiO_2 nanoparticles. The value of the diffusion coefficient of Li^+ ion was ordered: TiO_2@C-2 > TiO_2@C-3 > TiO_2@C-1 > TiO_2. These results of the EIS confirm the hypothesis that nitrogen-doping can improve the ion permeability of the carbon shell and the charge transfer at the interface, which will be favorable for the electrochemical performance of lithium-ion battery during cycling. It also can be found that the thickness of the carbon layer directly affected the value of the diffusion coefficient of the TiO_2@C electrodes. The highest value of the diffusion coefficient is obtained for the carbon layer with 4 nm.

Due to lowest charge transfer resistance and highest the diffusion coefficient of Li^+ ion, TiO_2@C-2 with the carbon layer thickness of 4 nm shows best performance based on high capacity and good cyclability among the TiO_2@C electrodes in our experiments. From Fig. 6, it can also be found that the capacity retention of TiO_2@C-3 electrode (99% after 170th cycles) was much higher than that of both TiO_2@C-1 (81.8% after 170th cycles) and TiO2@C-2 (88.5% after 170th cycles) electrodes. The capacity of TiO_2@C-3 electrode (131.4 mAh g^{-1} after 170th cycles) was higher than that of TiO2@C-1 electrode (127.3 mAh g^{-1} after 170th cycles), however, much lower than that of TiO_2@C-2 electrode (142.4 mAh g^{-1}

Fig. 7. Discharge–charge profiles of TiO_2 and TiO_2@C nanocomposites for 170 cycles at 0.5 C. (a) TiO_2, and TiO_2@C nanocomposites as the self-polymerization of dopamine for 5 h (b), 10 h (c) and 24 h (d), respectively.

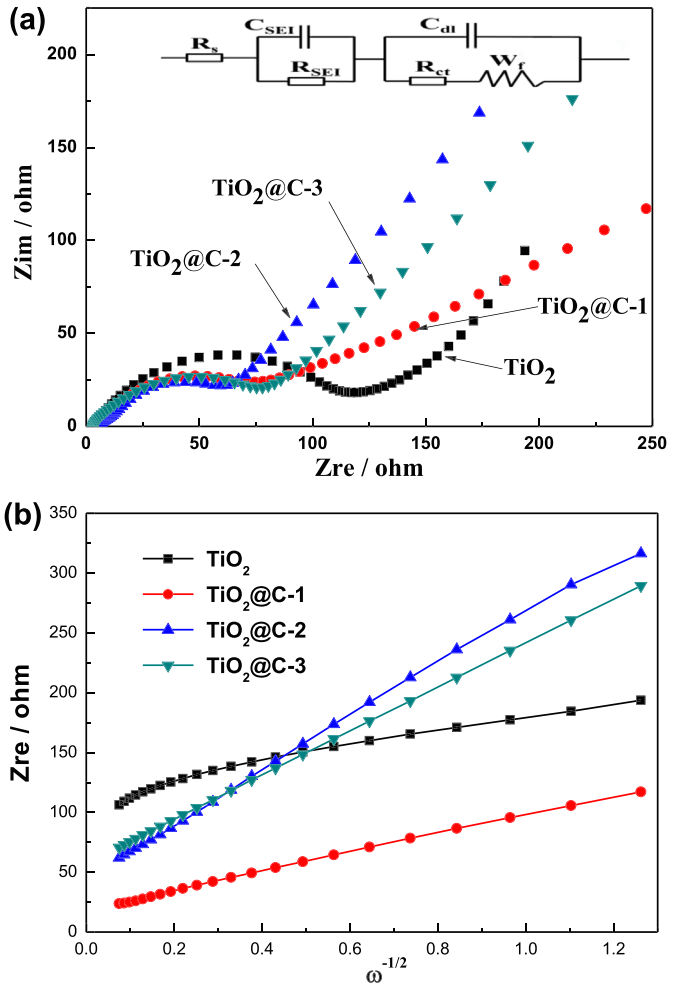

Fig. 9. Nyquist plots of TiO_2 and TiO_2@C electrodes after 170th cycles.

after 170th cycles). We think the main reason of these behavior on the capacity retention and specific capacity as a function of cycle number is the thickness of carbon layers. A carbon layer with appropriate thickness can buffer the TiO_2 nanoparticles growth during cycling, and ensure both elastic and good mechanical stability. When the carbon layer is too thin, smaller than 4 nm in our experiments (TiO_2@C-1), it is difficult to form a buffer layer which is strong enough to suppress the TiO_2 nanoparticle clustering and limit excessive TiO_2 particle growth (see Fig. 8c and d), which results in the capacity fading. Conversely, when the carbon layer is too thick, like TiO_2@C-3 with 6 nm thickness, the specific capacity of the TiO_2@C nanocomposites will decrease because of the restricted efficient ion transfer/transport (high charge transfer resistance and low the diffusion coefficient of Li^+ ion). Therefore, the optimized thickness of the carbon layer on the anatase TiO_2 nanoparticles should be about 4–5 nm in our experiments.

4. Conclusions

In order to improve the cycling performance of anatase TiO_2 nanoparticles, nitrogen-doped carbon coated TiO_2 composites were prepared by using polydopamine as carbon precursor. Due to the protective effect of the conductive N-doped carbon coating layer, the lithium-ion battery using TiO_2@C nanocomposites as anode shows good cyclability and high capacity compared with the pristine TiO_2. Since dopamine can be coated on virtually any surface with good thickness controlled, it can also be extended to develop new TiO_2@C composites materials based on various polymorphs (rutile, anatase and brookite) or nanostructures (such as nanotube, nanowire or nanosheet) of TiO_2 for lithium-ion battery, supercapacitor, solar cell, gas sensing and environmental applications.

Acknowledgments

The work was supported by the National Natural Science Foundation of China (20904031), and Shanghai key lab of polymer and electrical insulation (Shanghai key lab of electrical insulation and thermal aging). Thanks for Instrumental Analysis Center of Shanghai Jiaotong University.

References

[1] G.N. Zhu, Y.G. Wang, Y.Y. Xia, Energy Environ. Sci. 5 (2012) 6652.
[2] B. Scrosati, J. Garche, J. Power Sources 195 (2010) 2419.
[3] M.M. Rahman, J.Z. Wang, D. Wexler, Y.Y. Zhang, X.J. Li, S.L. Chou, H.K. Liu, J. Solid State Electrochem. 14 (2010) 571.
[4] M.G. Kim, H. Kim, J. Cho, J. Electrochem. Soc. 157 (2010) 802.
[5] J. Xu, Y. Wang, Z. Li, W.F. Zhang, J. Power Sources 175 (2008) 903.
[6] H. Qiao, L. Xiao, L. Zhang, Electrochem. Commun. 10 (2008) 616.
[7] J. Jamnik, R. Dominko, B. Erjavec, M. Remskar, A. Pintar, M. Gaberscek, Adv. Mater. 21 (2009) 271.
[8] S.-J. Park, Y.-J. Kim, H. Lee, J. Power Sources 196 (2011) 5133.
[9] X. Zhang, H. Li, X. Cui, Y. Lin, J. Mater. Chem. 20 (2010) 2801.
[10] K.S. Raja, M. Misra, V.K. Mahajan, T. Gandhi, P. Pillai, S.K. Mohapatra, J. Power Sources 161 (2006) 1450.
[11] L.W. Su, Y.R. Zhong, J.P. Wei, Z. Zhou, RSC Adv. 3 (2013) 9035.
[12] L.W. Su, Y. Jing, Z. Zhou, Nanoscale 3 (2011) 3967.
[13] Y.F. Li, Z. Zhou, P.W. Shen, Z.F. Chen, Chem. Commun. 46 (2010) 3672.
[14] L.W. Su, Z. Zhou, P.W. Shen, Electrochim. Acta 87 (2013) 180.
[15] H. Lee, S.M. Dellatore, W.M. Miller, P.B. Messersmith, Science 318 (2007) 426.
[16] L. Zhao, Y.S. Hu, H. Li, Z.X. Wang, L.Q. Chen, Adv. Mater. 23 (2011) 1385.
[17] J. Hao, L. Yang, C. Li, C. Yan, P.S. Lee, J. Ma, Energy Environ. Sci. 4 (2011) 1813.
[18] C. Lei, F. Han, D. Li, W.C. Li, Q. Sun, X.Q. Zhang, A.H. Lu, Nanoscale 5 (2013) 1168.
[19] L. Tan, C. Cao, H. Yang, B. Wang, L. Li, Mater. Lett. 109 (2013) 195.
[20] Z. Xi, Y. Xu, L. Zhu, Y. Wang, B. Zhu, J. Membr. Sci. 327 (2009) 244.
[21] V.G. Pol, A. Zaban, Langmuir 23 (2007) 11211.
[22] J.H. Kong, W.A. Yee, L.P. Yang, Y.F. Wei, S.L. Phua, H.G. Ong, J.M. Ang, X. Li, X.H. Lu, Chem. Commun. 48 (2012) 10316.
[23] L.W. Su, Z. Zhou, P.W. Shen, J. Phys. Chem. C 116 (2012) 23974.
[24] M.M. Zhen, L.W. Su, Z.H. Yuan, L. Liu, Z. Zhou, RSC Adv. 3 (2013) 13696.
[25] Q. Cao, H.P. Zhang, G.J. Wang, Q. Xia, Y.P. Wu, H.Q. Wu, Electrochem. Commun. 9 (2007) 1228.
[26] A.Y. Shenouda, H.K. Liu, J. Power Sources 185 (2008) 1386.